Available online at www.sciencedirect.com
ScienceDirect
Remote Sensing of Environment 109 (2007) 166–182
Remote Sensing of Environment
www.elsevier.com/locate/rse

Coupled soil–leaf-canopy and atmosphere radiative transfer modeling to simulate hyperspectral multi-angular surface reflectance and TOA radiance data

Wout Verhoef [a,*], Heike Bach [b]

[a] National Aerospace Laboratory NLR, P.O. Box 153, 8300 AD Emmeloord, The Netherlands
[b] VISTA Geowissenschaftliche Fernerkundung GmbH, Gabelsbergerstraße 51, D-80333 Munich, Germany

Received 25 August 2006; received in revised form 20 December 2006; accepted 22 December 2006

Abstract

Coupling radiative transfer models for the soil background and vegetation canopy layers is facilitated by means of the four-stream flux interaction concept and use of the adding method. Also the coupling to a state-of-the-art atmospheric radiative transfer model like MODTRAN4 can be established in this way, thus enabling the realistic simulation of top-of-atmosphere radiances detected by space-borne remote sensing instruments. Possible applications of coupled modeling vary from mission design to parameter retrieval and data assimilation. This paper introduces a modified Hapke soil BRDF model, a robust version of the PROSPECT leaf model, and a modernized canopy radiative transfer model called 4SAIL2. The latter is a hybrid two-layer version of SAIL accommodating horizontal and vertical heterogeneities, featuring improved modeling of the hot spot effect and output of canopy absorptances. The integrated model is simply called SLC (soil–leaf-canopy) and has been implemented as a speed-optimized Windows DLL which allows efficient use of computer resources even when simulating massive amounts of hyperspectral multi-angular observations. In this paper various examples of possible model output are shown, including simulated satellite image products. First validation results have been obtained from atmospherically corrected hyperspectral multi-angular CHRIS-PROBA data of the Upper Rhine Valley in Germany.

Keywords: Coupled radiative transfer models; Hyperspectral multi-angular observations; TOA radiance; Canopy reflectance; CHRIS-PROBA

1. Introduction

Optical remote sensing methods to observe and monitor the status of vegetation canopies have been in use since airborne and space-borne electronic sensing devices moved into regular operation in the early 1970s. Since that time also the modeling of vegetation radiative transfer (Allen et al., 1970; Suits, 1972) has been recognized as an important tool to better understand and quantify the relationships between vegetation object properties and remotely detected radiance signals. The bi-directional reflectance, or rather the bi-directional reflectance distribution function BRDF (Nicodemus, 1970), of vegetation canopies is the fundamental physical object property which eventually determines the remotely sensed radiance signal, along with other factors such as the local solar and sky irradiances, and the atmospheric conditions. Modeling the top-of-canopy BRDF has evolved in several directions (Goel, 1988; Pinty et al., 2004), making use of various numerical solution techniques like ray tracing (Chelle, 1997), Monte Carlo (North, 1996; Thompson & Goel, 1998) and radiosity (Gerstl & Borel, 1992), or analytical solutions like four-stream (Verhoef, 1985), $N+2$ stream (Verhoef, 2002) and discrete ordinates (Knyazikhin et al., 1992), for 1-D as well as 3-D canopy architectures (Gastellu-Etchegory et al., 1996; Kuusk & Nilson, 2000). In hybrid models analytical and numerical techniques are combined (Gobron et al., 1997), or geometric optics (GO) approaches are combined with radiative transfer (RT) approaches (so-called GORT models, Li et al., 1995). Depending on the field of application, some models may put much emphasis on the internal numerical accuracy, 3-D radiation transport (Shultis & Myneni, 1988) and the 3-D canopy architecture, others might pay more attention to the detailed

* Corresponding author. Tel.: +31 527 24 82 53; fax: +31 527 24 82 10.
E-mail address: verhoef@nlr.nl (W. Verhoef).

0034-4257/$ - see front matter © 2007 Elsevier Inc. All rights reserved.
doi:10.1016/j.rse.2006.12.013

spectral effects of leaf biochemistry or to the directional scattering of radiation by particular model elements, *e.g.* shoots in a coniferous forest canopy (Smolander & Stenberg, 2003). Numerical techniques such as ray tracing are particularly useful to investigate photon transport in complex media, and 3-D models have been designed to incorporate landscape heterogeneity. However, reality is always more complex than any model is able to capture, so in practice one has to work with model abstractions, simplifications and approximations. Frequently applied simplifications are the assumption of bi-Lambertian reflection and transmission of radiation from leaves or needles, Lambertian soil reflection, and of the spectral homogeneity of phytoelements and soil. Elements like stems and branches are often ignored. From the point-of-view of model inversion there is general consensus that invertible models should not contain too many parameters, since otherwise the model inversion becomes unstable and ill-posed (Combal et al., 2002; Nilson & Kuusk, 1989). Yet models should be realistic enough to capture the most prominent spectral BRDF effects occurring in nature. So a compromise has to be sought between model simplicity and realism.

Top-of-atmosphere radiance observations of vegetation canopies are influenced by the optical properties of the atmosphere, by the soil or understorey background, and by the optical and structural properties of the vegetation itself, which can be decomposed into phytoelements like leaves or needles, and other structural entities like shoots, twigs, branches, trunks, stems, heads, ears and flowers. All of these elements have the potential of becoming important in particular situations, so a model should accommodate at least a number of these elements and include effects that are expected to have a significant impact on the observations. Therefore it is considered essential to spread attention as much as possible over different potential influences originating from the atmosphere, the soil background, leaf biochemistry and canopy architecture. For instance, a model which pays much attention to 3-D canopy architecture, but ignores the anisotropy of the soil BRDF, might perform worse than a less sophisticated model that spreads attention over both effects. The canopy radiative transfer model that underlies the NASA LAI/FPAR algorithm accounts for soil anisotropy, non-Lambertian surface, canopy 3D effects and simulates canopy spectral response (Knyazikhin et al., 1998).

Four-stream radiative transfer theory (Verhoef, 1985; Verhoef & Bach, 2003) provides a particularly useful framework to facilitate the flexible coupling of models for the soil BRDF, the canopy layer, and the atmosphere. In this paper an integrated radiative transfer model is presented which is meant to simulate top-of-canopy spectral reflectance observations of soil-vegetation ensembles under a wide range of circumstances. It is simply called SLC (soil–leaf-canopy) and consists of a modified Hapke (1981) soil BRDF model, a robust version of the PROSPECT leaf optical properties model (Jacquemoud & Baret, 1990), and the canopy radiative transfer model 4SAIL2, a two-layer robust version of SAILH (i.e. SAIL including hot spot effect) which incorporates crown clumping effects so that it may also accommodate the modeling of forests. The 4SAIL2 model contains elements from predecessors like FLIM (crown clumping; Rosema et al., 1992), GeoSAIL (vertical leaf color gradient; Verhoef & Bach, 2003) and SAIL++ (numerical robustness; Verhoef, 2002). It includes an improved modeling of the hot spot effect, and provides canopy absorption spectra as output. More details are given in Section 2. In Section 3 a couple of examples of the functioning of the model and of its use are demonstrated. First validation results for the model based on atmospherically corrected multi-angular CHRIS-PROBA data of the Upper Rhine Valley in Germany are presented in Section 4.

2. Models and methods

2.1. Modified Hapke model including soil moisture effect

Many soil-canopy radiative transfer models assume that the soil background can be treated like a Lambertian reflector. However, especially for sparse vegetation canopies this assumption may lead to serious deviations from actual top-of-canopy bi-directional reflectance measurements. Therefore, in SLC a soil BRDF model has been incorporated in which the interaction with the canopy layer is described by means of four-stream radiative transfer equations. The basis of this model is formed by Hapke's soil model (Hapke, 1981), which describes scattering inside the soil medium by means of a scattering phase function which is parameterized as a second-order Legendre polynomial, and which includes a hot spot correction term in the single scattering contribution to the computed bi-directional reflectance (Pinty et al., 1989). For the calculation of the multiple scattering contribution in the Hapke model it is assumed that scattering is isotropic. However, this assumption proves to be not necessary, so it was decided to modify the original model by using the complete non-isotropic phase function instead. Also in the directional-hemispherical reflectances and the bi-hemispherical reflectance computed by the new model (which are necessary for the interaction with the canopy layer) the full original phase function is still applied, so that the internal consistency of the model as a whole has improved. The scattering phase function $p(\delta)$ is described as a second-order Legendre polynomial with two parameters b and c as follows:

$$p(\delta) = 1 + b\cos\delta + c(\cos^2\delta - 1)/2$$

where δ is the scattering angle. The single scattering contribution to the bi-directional reflectance is given by (Pinty et al., 1989)

$$r^s_{so} = \frac{\omega}{4}\frac{1 + B(\delta)}{\mu_s + \mu_o}p(\delta)$$

where ω is the single scattering albedo and μ_s and μ_o are the cosines of the solar zenith angle and the observer's zenith angle, respectively. The term $B(\delta)$ is responsible for the soil's hot spot effect and is given by

$$B(\delta) = \frac{B_0}{1 + \frac{\tan(\delta/2)}{h}}$$

Here, B_0 describes the relative magnitude of the hot spot peak, while h controls its (half) width. The total number of

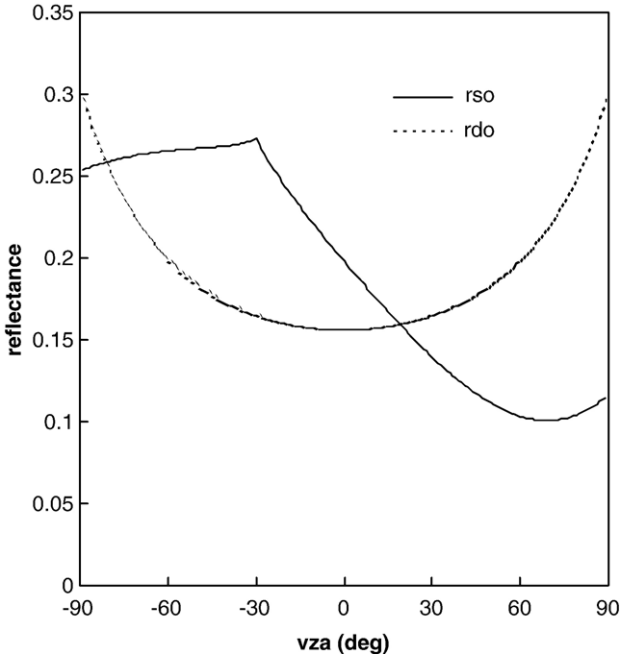

Fig. 1. Soil reflectance in the principal plane as simulated by the modified Hapke soil BRDF model. Shown are the directional reflectances for solar flux (r_{so}) and for diffuse incident flux (r_{do}) at 670 nm for a solar zenith angle of 30°.

parameters of the Hapke model is five, of which two (ω and b) affect all reflectance factors, and three (B_0, h and c) only have an influence on the bi-directional reflectance. In the current implementation of the model only the single scattering albedo is assumed to be spectrally dependent.

In order to simulate the effect of soil moisture on the soil's reflectance, use is made of a physically based model described in Bach and Mauser (1994). This model considers the two main effects of liquid water on the soil's reflectance, namely the effect of a water film on soil particles, which gives a spectrally almost uniform decrease of the reflectance, and the additional effect of specific absorption by water, which is spectrally highly variable. Since this model considers only hemispherical fluxes, only the effect of moisture on the bi-hemispherical reflectance is predicted in principle. However, it is obvious that, in order to extend the effect to all four 4-stream reflectance factors, one has to modify the single scattering albedo, after which the soil model can be applied again in forward direction in order to obtain all four moisture-affected reflectance factors. The relationship between the single scattering albedo and the bi-hemispherical reflectance is quite simple and given by

$$r_{dd} = \frac{1-\sqrt{\frac{1-\omega}{1+1/4\omega b}}}{1+\sqrt{\frac{1-\omega}{1+1/4\omega b}}},$$

and for given b one can easily find the inverse relationship

$$\omega = \frac{1-\left(\frac{1-r_{dd}}{1+r_{dd}}\right)^2}{1+1/4b\left(\frac{1-r_{dd}}{1+r_{dd}}\right)^2}.$$

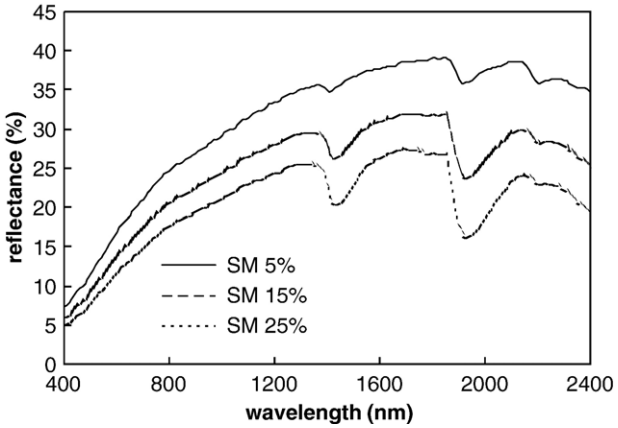

Fig. 2. Modeling the effect of an increasing soil moisture (volumetric percentage) on the soil's bi-directional reflectance spectrum.

This inverse relationship is used to convert the moisture-affected spectrum of the bi-hemispherical reflectance into a moisture-affected spectrum of the soil single scattering albedo. The Hapke soil model has been validated by Pinty et al. (1989). In Bach (1995) several examples are given of successful validations of the soil moisture effect for common soil types.

One example of soil BRDF effects simulated with the new model is illustrated in Fig. 1. It shows the directional reflectances in the principal plane for direct sunlight and for diffuse (hemispherical and isotropic) incident flux at 670 nm and for a solar zenith angle of 30°. In this case the Hapke parameters were set equal to their default values, which have been taken from the values that Pinty et al. (1989) obtained for a ploughed soil, namely $b=0.84$; $c=0.68$; $B_0=0.30$; $h=0.23$. These settings create a substantial directional variation in both reflectances, including a very wide hot spot effect in the bi-directional reflectance. However, this is not uncommon for

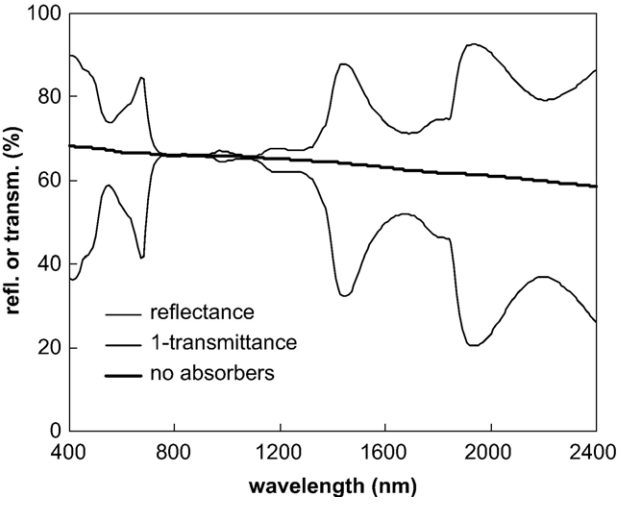

Fig. 3. Sample reflectance/transmittance spectra calculated by a robust version of the PROSPECT leaf model for $N=3$. Transmittance is shown from top to bottom. The middle curve (thicker line) is for no absorbers at all. For the other situation $C_{ab}=5$ μg/cm^2 and $C_w=0.01$ g/cm^2.

Table 1
Summary of SAIL family of canopy reflectance models

Property/model	SAIL	SAILH	GeoSAIL	SAIL++	4SAIL	4SAIL2
Year of development	1981	1989	1999	2000	2003	2003
Type	Turbid medium	Hybrid	Hybrid	Hybrid	Hybrid	Hybrid
Hot spot effect	No	Yes	Yes	Yes	Yes	Yes
# of canopy layers	1	1	2	1	1	2
Singularity removal	No	No	No	Yes	Yes	Yes
Numerical precision	Single	Single	Single	Double	Double	Single
Speed optimization	No	No	No	Yes	Yes	Yes
# of diffuse streams	2	2	2	72	2	2
Internal flux profiles supported	No	No	No	No	Yes	No
Thermal application supported	No	No	No	No	Yes	No
Non-Lambertian soil BRDF	No	No	No	No	No	Yes
Crown clumping effects	No	No	No	No	No	Yes

soils, which do not have the fine internal shadowing effects that are often seen in vegetation canopies.

An example of the modeled soil moisture effect on the soil's reflectance spectrum is shown in Fig. 2. This shows that from what is considered the dry situation, with a volumetric soil moisture content of 5%, the reflectance decreases overall, but more in the water absorption bands around 1450 and 1950 nm, as expected.

2.2. PROSPECT

The leaf radiative transfer model PROSPECT has been validated and applied in numerous studies (Le Maire et al., 2004; Zarco-Tejada et al., 2003), and in combination with canopy reflectance models it has been successfully applied in order to investigate the effects of leaf constituents and properties on optical observations at the canopy level (Bacour et al., 2002). Incorporation of the model in a chain of coupled models can be very useful, especially for parameter retrieval by model inversion. In SLC a version of PROSPECT is incorporated that handles the case of conservative scattering by employing a particular solution to the Stokes equations in order to estimate leaf reflectance and transmittance, thus improving the numerical robustness of the model. In PROSPECT the Stokes equations are applied in order to determine the reflectance and transmittance of $N-1$ elementary plates from those of a single elementary plate (Jacquemoud & Baret, 1990). If the latter are called r and t, respectively, then one can compute r_{N-1} and t_{N-1} by application of the Stokes equations. These equations fail in the case of conservative scattering, which leads to numerical problems under the condition $r+t=1$. However, by referring to a two-stream approximation for this particular situation and applying the appropriate limit, it turns out to be possible to recover this case. The solution is given by

$$t_{N-1} = \frac{1}{1+\frac{r}{t}(N-1)} = \frac{t}{t+(1-t)(N-1)}, \text{with } r_{N-1} = 1-t_{N-1}.$$

In Fig. 3 samples of leaf spectra calculated with the robust model for $N=3$ are shown for the case of no absorbers at all and for small concentrations of chlorophyll a,b (C_{ab}) and leaf water, C_w. In the case of no absorption the spectral variation left is only due to the weak variation of the index of refraction with wavelength, which gives a slowly decreasing reflectance along with an increasing transmittance, such that their sum remains one.

2.3. The 4SAIL2 model

2.3.1. Historic notes

The model 4SAIL2 is a recent version of the SAIL model (Verhoef, 1984, 1998) which features a number of improvements compared to earlier versions of the model. The name has been chosen to reflect its intensive use of four-stream radiative transfer concepts, and the fact that it is a two-layer model. For the optical interaction with a non-Lambertian soil background, and for the interactions between both canopy layers, as well as for the calculation of the effective top-of-canopy reflectance quantities, use is made of the four-stream adding method (Van de Hulst, 1980; Verhoef, 1985; Verhoef & Bach, 2003). The two-layer structure has been devised in order to accommodate a vertical leaf color gradient, as often seen in canopies like wheat. This is similar to the GeoSAIL model, which was briefly introduced in Verhoef and Bach (2003). Note that GeoSAIL should not be confused with a hybrid model named GeoSail (Huemmrich, 2001), which is based on SAIL and includes Jasinski's parameterization of crown clumping (Jasinski, 1996). Table 1 shows a functional overview of the most relevant members of the SAIL family of canopy reflectance models, including a number of typical characteristics of each. From this summary it can be observed that 4SAIL2 inherits its two-layer structure from GeoSAIL, and singularity removal and speed optimization from SAIL++ (Verhoef, 2002). The original SAIL model is the only pure turbid medium model of Table 1. All other models include the hot spot effect, which is connected to the finite size of the leaves, and recently also geometric crown clumping effects, so all later models fall in the category hybrid. New in 4SAIL2 is the incorporation of a non-Lambertian soil BRDF, as well as crown clumping effects like in forests. Regarding Table 1, it should be mentioned that the model 4SAIL, which is a (yet unpublished) modernized single-layer version of SAILH, has been in use for some time already for *e.g.* thermal applications and to obtain internal radiation profiles for canopy fluorescence modeling. However, this falls outside the scope of the present contribution and here only the new features of 4SAIL2 will be discussed in some more detail.

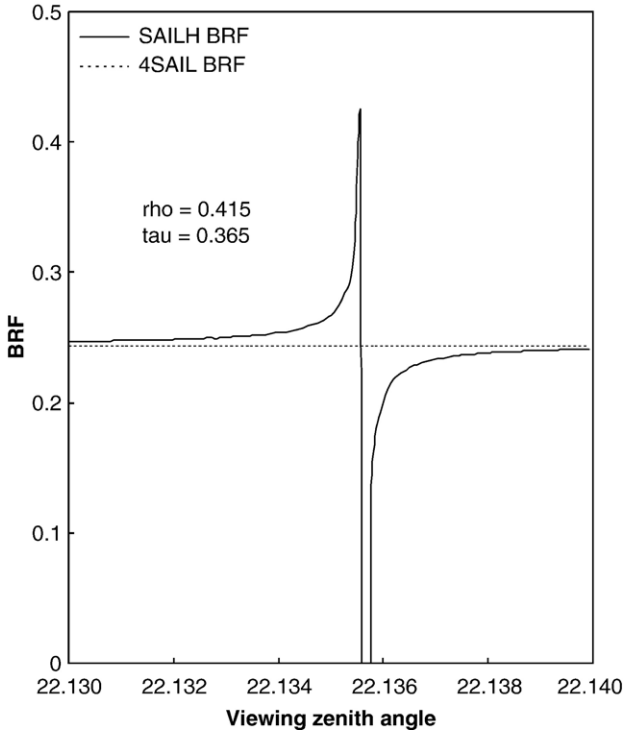

Fig. 4. Numerical instability in SAILH model and corresponding smooth BRF output of model 4SAIL in which this singularity is properly intercepted. Rho and tau indicate single leaf reflectance and transmittance.

2.3.2. Singularity problem

Radiative transfer models that are solved analytically by means of eigenvector decomposition are susceptible to numerical inaccuracy related to mathematical singularities (Verhoef, 1998) caused by duplicate eigenvalues. In four-stream models with two direct fluxes and two hemispherical diffuse fluxes such as the SAIL models (except SAIL++) the eigenvalues are given by m, $-m$, k and K, where the former two are related to the upward and downward diffuse fluxes, and the latter two are the extinction coefficients for direct solar flux and for radiance in the viewing direction, respectively. In general, four singular cases are possible, namely

I. $m=-m$
II. $k=m$
III. $K=m$
IV. $K=k$.

Case I implies $m=0$ and occurs for conservative scattering (zero absorption), in which case also the eigenvalue associated with the diffuse flux system equals zero. Although in practice this case does not occur in vegetation canopies, since leaves will always absorb some radiation (even in the near infrared), it is still being intercepted in 4SAIL2 because the robust version of PROSPECT discussed in Section 2.2 has been given the ability to handle this case, so the canopy model should be capable of handling it as well.

Cases II and III are the most common ones encountered in practice, since there will often be a particular wavelength where the spectral properties of the leaves are such that $m=k$ or $m=K$. Especially with hyperspectral modeling applications there is a fair chance that these conditions will occur, or at least are closely approximated. The eigenvalue m is related to the absorption coefficient of the medium, and therefore spectrally highly variable, whereas both extinction coefficients are only direction-dependent. This implies that especially with hyperspectral multi-angular simulations one may encounter spectral-directional combinations for which this condition occurs. And it will be obvious that also parameter retrieval by model inversion cannot be based on a numerically unstable radiative transfer model, so a proper interception of these conditions was considered essential.

Case IV happens when the zenith angles of observation and the sun are equal, such as for instance in the hot spot. This case has been analyzed in Verhoef (1998), but fortunately it has only consequences for the calculation of the layer's bi-directional transmittance, a quantity which for observation of vegetation canopies from above is not very relevant, so it is further ignored.

Interception of these special cases could be carried out by analyzing them mathematically and replacing the expressions valid for the normal case by expressions that are specifically valid for the corresponding particular solution. However, it turns out that this is not sufficient, since the problem is not so much what happens when the singularity holds exactly, but rather what happens in the near proximity of it. Strictly speaking this is not a singular case, so the normal expressions would still be valid, but applying these will create numerical problems

Table 2
Four-stream optical quantities for a 2-layer homogeneous vegetation canopy medium

Optical quantity	Description
ρ_{dd}^{t}	Bi-hemispherical reflectance at top-of-canopy
ρ_{dd}^{b}	Bi-hemispherical reflectance at bottom-of-canopy
τ_{dd}	Bi-hemispherical transmittance
ρ_{sd}	Directional-hemispherical reflectance for solar flux
τ_{sd}	Directional-hemispherical transmittance for solar flux
ρ_{do}	Hemispherical-directional reflectance in viewing direction
τ_{do}	Hemispherical-directional transmittance in viewing direction
τ_{ss}	Direct transmittance for solar flux
τ_{oo}	Direct transmittance in viewing direction
ρ_{so}	Bi-directional reflectance
τ_{ssoo}	Bi-directional gap probability

Table 3
Modulation of canopy layer optical quantities by clumping effects

Optical quantity	Modulation by clumping parameters
ρ_{dd}^{t}	$C_v\rho_{dd}^{t}$
ρ_{dd}^{b}	$C_v\rho_{dd}^{b}$
τ_{dd}	$(1-C_v)+C_v\tau_{dd}$
ρ_{sd}	$C_s\rho_{sd}$
τ_{sd}	$C_s\tau_{sd}$
ρ_{do}	$C_o\rho_{do}$
τ_{do}	$C_o\tau_{do}$
τ_{ss}	$(1-C_s)+C_s\tau_{ss}$
τ_{oo}	$(1-C_o)+C_o\tau_{oo}$
ρ_{so}	$(1-F_{os})\rho_{so}$
τ_{ssoo}	$F_{cd}\tau_{ssoo}+F_{cs}\tau_{oo}+F_{od}\tau_{ss}+F_{os}$

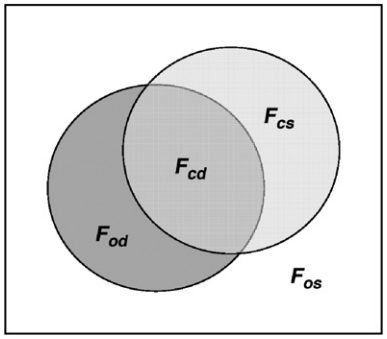

Fig. 5. Crown projections from the directions of the sun and viewing, and the associated four area fractions on the background surface.

since they will become very inaccurate in the neighborhood of a singularity. This is illustrated in Fig. 4, which shows the bi-directional reflectance factor (BRF) as calculated with the older model SAILH compared to the one calculated with the modernized model 4SAIL. In the latter model the proper interception of singular cases II and III has been applied. In this particular example the viewing zenith angle is varied over a very small range, and about halfway this range the condition $K=m$ (equality of the extinction coefficient in the viewing direction to the positive eigenvalue of the diffuse flux system) is encountered. It turns out here that the model SAILH exhibits a large fluctuation caused by numerical instability, whereas the new model output remains perfectly smooth across the entire range. Note, that even negative calculated reflectances can be the result of this phenomenon.

It turns out that the cause of the numerical instabilities can always be traced back to functions of the type

$$J = \frac{\exp(-bL)-\exp(-aL)}{a-b},$$

which appear in the analytical solution of the four-stream system of radiative transfer equations. If a and b are two eigenvalues and L is the leaf area index, then calculation of the function J in a computer becomes extremely inaccurate if both eigenvalues are nearly equal. When both are exactly equal, the mathematical solution is simply given by the limit $J|_{a=b}=L\exp(-aL)$. In the neighborhood of the singularity (small $\varepsilon=a-b$) one should better apply the very accurate and numerically stable expression

$$J = \frac{\exp(-aL)+\exp(-bL)}{2} L\left[1-\frac{1}{12}(a-b)^2L^2\right].$$

In practice this approximation is applied for values of $|\varepsilon|<10^{-3}$, which is sufficient to gracefully circumvent any numerical instability due to duplicate eigenvalues. In the example of Fig. 4 the single leaf reflectance and transmittance values are 0.415 and 0.365, respectively, which for green vegetation typically can be found in the transition from the red to the near infrared part of the spectrum. This case has been reconstructed from a practical simulation of a barley canopy at the Barrax site in Spain (Verhoef & Bach, 2003) which had been carried out with the GeoSAIL model.

2.3.3. Crown clumping

Crown clumping can be modeled as local accumulations of foliage such as in forest stands. Although in real forests clumping may occur simultaneously on various levels of aggregation (i.e. shoots, branches, whole crowns), only the clumping on crown level is considered in 4SAIL2. In this model two parameters are used to characterize crown clumping, namely the vertical crown cover percentage C_v (the percentage of ground area covered with crowns as seen from nadir direction), and a tree shape factor ξ. The latter is defined as the ratio of crown diameter to crown height (i.e. the height of the crown's center above the ground). Both parameters are used in a semi-empirical manner in order to modulate the optical output parameters of the homogeneous model, which consist of eleven reflectance and transmittance factors. In the semi-empirical Forest Light Interaction Model (FLIM) of Rosema et al. (1992) a similar parameterization was applied to the single scattering contributions from crowns and soil or understorey background. However, in that model both crowns and soil were assumed to reflect the incident radiation isotropically, whereas in 4SAIL2 the bi-directional properties of foliage and background are fully integrated. The effective eleven optical quantities of a horizontally homogeneous canopy medium consisting of two sub-layers are summarized in Table 2. In Table 3 it is shown how these quantities are modulated by the clumping effect. The applied modulation is based on the principle of linearly mixing the reflectances and transmittances of the homogeneous canopy with those of empty space, using the appropriate area fractions as weights. Linear mixing as applied here ignores mutual scattering between tree crowns (Asrar et al., 1992), but shadowing effects on the soil background are taken into account. In Table 3 all reflectances of empty space are taken to be zero, whereas the associate transmittances are also zero, unless a direct transmittance (i.e. one without scattering) is included, in which case the transmittance of open space is taken

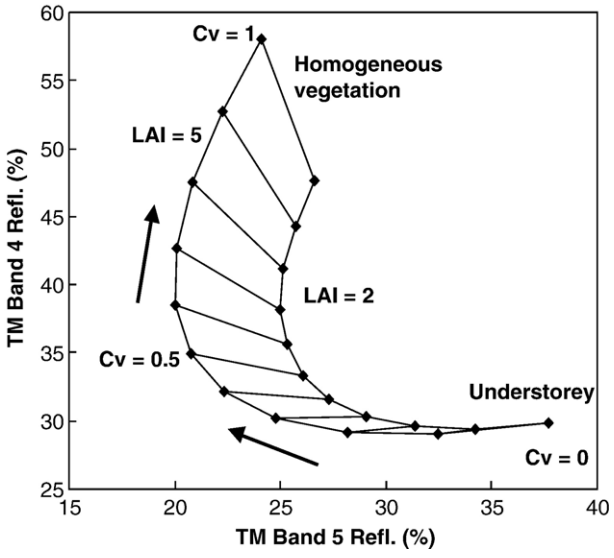

Fig. 6. Variation of fractional crown cover from zero to one plotted in the TM band 5/band 4 feature space for LAIs of 2 and 5, as simulated with 4SAIL2 model. The arrows indicate increasing crown cover.

to be equal to one. The latter applies to τ_{dd}, τ_{ss}, and τ_{oo}. A second principle which has been followed is that of maintaining symmetry between solar incidence and viewing, so that the reciprocity relations remain intact. Therefore, after applying the modulations due to clumping, all optical quantities of the canopy layer still obey the fundamental reciprocity laws.

In total, 7 clumping-related area fractions can be identified, which are described as follows:

C_v vertically projected crown cover fraction
C_s crown cover fraction projected in the direction of the sun
C_o crown cover fraction projected in the direction of viewing
F_{cd} ground area fraction obscured by crowns from viewing and in the shade
F_{cs} ground area fraction obscured by crowns from viewing and in the sun
F_{od} viewed ground open space fraction between trees in the shade
F_{os} viewed ground open space fraction between trees in the sun

The last four (F-) fractions are illustrated in Fig. 5 for a single crown envelope. With respect to the paper of Rosema et al. (1992) the F-fractions have been corrected so as to prevent exceeding the maximum possible spatial correlation between the projections of crowns on the ground in the directions of the sun and of viewing. This is accomplished by redefining the overlapping area fraction O to the modified expression

$$O = \min[C_s(1-C_o), C_o(1-C_s)]\exp(-\alpha/\xi)$$

where α the angular distance measure that is also used in the description of the foliage hot spot effect, i.e.

$$\alpha = \sqrt{\tan^2\theta_s + \tan^2\theta_o - 2\tan\theta_s\tan\theta_o\cos\psi} \quad .$$

Here θ_s, θ_o and ψ are the solar zenith angle, the observer zenith angle and the relative azimuth angle, respectively. As the tree shape factor ξ is usually much larger than the hot spot parameter of the foliage, two different hot spot effects will emerge from the new model: one relatively narrow hot spot related to the leaves or the needles, and one much wider hot spot related to crown shadowing on the background soil (see also Section 3.1). Considering in addition to this the possible hot spot effect of the non-Lambertian soil eventually leads to a composite hot spot effect in which all three can be mixed in various proportions depending on canopy architecture and LAI. In Section 3.1 some sample simulation results of this phenomenon will be shown. Here one sample simulation of the clumping effect is included in Fig. 6, showing the effects of increasing crown cover and LAI in a feature space plot of Landsat TM bands 4 and 5. In this case viewing is vertical and the solar zenith angle is 45°. The leaf inclination distribution function (LIDF) is spherical. It turns out that especially at intermediate crown cover fractions one obtains relatively low reflectances, which can be attributed to shadowing effects. Similar results were found by Rosema et al. (1992) with the FLIM model. This semi-empirical model has been validated on the basis of a large number of *in situ* observations in the Kootwijk forest (Douglas fir and Scots pine) in The Netherlands during five years and in several other studies (De Ruiter et al., 1997; Gemmell & Varjo, 1999). A clear difference between the models 4SAIL2 and FLIM is revealed at complete crown cover. In that case the output of FLIM forms a linear mixture between the understorey point and the dense forest point. With 4SAIL2 this mixing remains non-linear. The reason is that in 4SAIL2 internal crown radiative transfer is better taken into account, which comes to expression as a non-linear mixing of background and dense vegetation.

Table 4
Settings of LIDF parameters a and b to realize various LIDF types

LIDF type	a	b
Planophile	1	0
Erectophile	−1	0
Plagiophile	0	−1
Extremophile	0	1
Spherical	−0.35	−0.15
Uniform	0	0

The model INFORM (Atzberger, 2000; Schlerf & Atzberger, 2006) also takes as a basis the FLIM model and uses SAILH to compute crown reflectance and transmittance. For the foliage, both LIBERTY (Dawson et al., 1998) and PROSPECT can be taken as the single leaf or needle model. However, INFORM does not apply the clumping modulation to all optical properties of the canopy layer, and the reciprocity relations are not fully obeyed by this model.

2.3.4. Foliage hot spot

The foliage hot spot effect is based on the theory of Kuusk (1985), which employs the bi-directional gap probability function given by

$$P_{so}(x) = \exp[(K+k)Lx + \sqrt{Kk}L(1-e^{qx})/q]$$

where $q = \frac{\alpha}{s_{\mathscr{L}}}\frac{2}{K+k}$ is the factor that controls the width of the hot spot effect. Note that x is defined as the relative optical height inside the canopy layer, which by convention runs from −1 at the bottom to 0 at the top of the canopy. The foliage hot spot size parameter $s_{\mathscr{L}}$ is equal to the ratio of the correlation length of leaf projections in the horizontal plane and the canopy height. It should be emphasized here that the correction factor $2/(K+k)$ is applied in the more recent versions of the SAIL models in order to compensate the effect of shadow lengthening in the horizontal plane that occurs for inclined leaves at larger zenith angles (Bréon et al., 2002). Since the angular distance measure α is measured in the horizontal plane as well, compensation of shadow length in this way leads to a hot spot width that is less dependent on the zenith angle.

2.3.5. Implementation aspects

Calculation of the internal four-stream radiative transfer interactions required in order to combine both canopy layers, plus the coupling with the non-Lambertian soil background,

are all carried out inside the 4SAIL2 subroutine, in such a way that as output it provides four top-of-canopy reflectance factors and two canopy absorptances. These can be summarized as follows:

r^*_{so} bi-directional reflectance factor
r^*_{do} hemispherical-directional reflectance factor in viewing direction
r^*_{sd} directional-hemispherical reflectance factor for solar incident flux
r^*_{dd} bi-hemispherical reflectance factor
α^*_s canopy absorptance for direct solar incident flux
α^*_d canopy absorptance for hemispherical diffuse incident flux

The adding equations applied to calculate these quantities from the optical properties of the isolated canopy layer and the soil are given in Appendix A.

The order of working in applying the adding equations in 4SAIL2 to compute the TOC reflectances is as follows:

I Start with the isolated bottom canopy layer
II Add the top canopy layer and compute combined optical properties
III Apply modulations due to clumping
IV Add the soil surface at the bottom and compute TOC reflectances and absorptances.

Speed optimizations have been introduced by avoiding unnecessary repetition of calculations if only few parameters change between two successive calls. For instance, if only the wavelength changes, many geometrical calculations are needed only once and are bypassed after the first call, which speeds up execution significantly. The integrated model has been compiled as a Windows DLL (dynamically linked library) which can be called from several languages or environments. Successful demonstrations of application programs calling the DLL from Visual Basic 5, Java and Fortran have already been realized. On a 1.8 GHz PC the integrated SLC model, invoking calls to the soil BRDF model, the PROSPECT leaf model (twice, because of the green and brown leaves) and the canopy model 4SAIL2, is able to complete 70,000 full model runs (i.e. for one direction and one spectral band) per second, thus enabling its use in massive image simulation experiments or for model inversion.

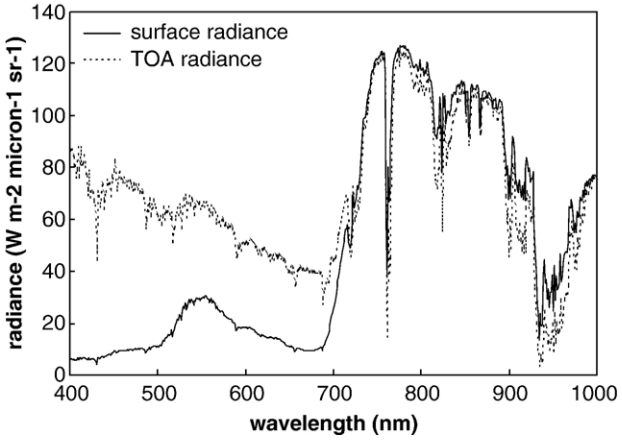

Fig. 7. Top-of-canopy and top-of-atmosphere radiance spectra at 1 nm resolution as computed by the coupled models 4SAIL and MODTRAN4 for a dense homogeneous canopy with LAI=4.

2.3.6. Model inputs

The required inputs of the model 4SAIL2 are summarized below:

Sun-object-sensor geometry
θ_s solar zenith angle
θ_o observation zenith angle
ψ relative azimuth angle

Leaf optical properties
ρ_g green leaf reflectance
τ_g green leaf transmittance
ρ_b brown leaf reflectance
τ_b brown leaf transmittance

Soil BRDF properties
r_{so} bi-directional reflectance factor
r_{do} hemispherical-directional reflectance factor in viewing direction
r_{sd} directional-hemispherical reflectance factor for solar incident flux
r_{dd} bi-hemispherical reflectance factor

Canopy architecture
LAI total (green + brown) leaf area index or total crown LAI for clumped vegetation
LIDFa LIDF parameter *a*, which controls the average leaf slope
LIDFb LIDF parameter *b*, which controls the distribution's bimodality
s_ℓ hot spot size parameter
f_B fraction brown leaf area
D layer dissociation factor
C_v vertical crown cover percentage
ξ tree shape factor

The two LIDF parameters are used in more recent models (Verhoef, 1998) in order to shape the LIDF with great flexibility. Table 4 shows a number of settings of these parameters in order to obtain some well-known leaf angle distributions found in the literature. The spherical distribution cannot be reproduced exactly by this parameterization, but a close approximation can be realized by means of the given combination of parameters.

2.4. Coupling with the atmosphere

The directional reflectance factor (DRF) as measured on the ground by using a white Lambertian diffusing panel as a

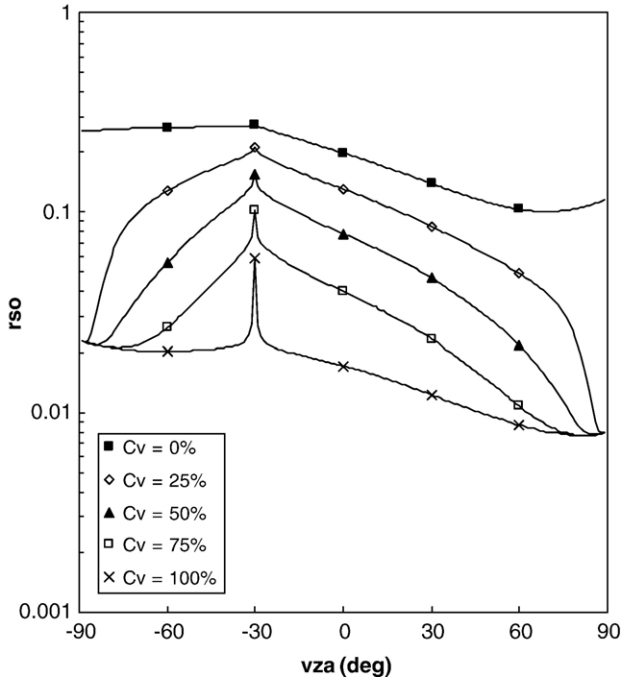

Fig. 8. Bi-directional reflectance (logarithmic scale) in the principal plane at 670 nm, demonstrating the mixing of distinct hot spot effects due to (1) the soil BRDF, (2) crown clumping, and (3) crown foliage. Crown LAI is always 4 in this case.

calibration reference is always a mixture of the reflectance responses for direct solar incident flux and for hemispherical diffuse incident flux from the sky. Therefore, in general the atmosphere always has some influence on measured surface reflectance values. And since in turn the sky irradiance to a small extent depends on the average surface reflectance of the surroundings, the measured DRF is even slightly influenced by the surroundings. As explained in Verhoef and Bach (2003), by means of four-stream radiative transfer equations, the interaction between the surface BRDF properties of the landscape and six effective optical parameters of the atmosphere can be conveniently described, which leads to the following set of equations.

$$E_{\mathrm{sun}} = \tau_{\mathrm{ss}}^{\mathrm{a}} E_{\mathrm{s}}^{\mathrm{o}} \cos\theta_{\mathrm{s}} \tag{1}$$

$$E_{\mathrm{sky}} = \frac{\tau_{\mathrm{sd}}^{\mathrm{a}} + \tau_{\mathrm{ss}}^{\mathrm{a}} \overline{r_{\mathrm{sd}}^{*}} \rho_{\mathrm{dd}}^{\mathrm{a}}}{1 - \overline{r_{\mathrm{dd}}^{*}} \rho_{\mathrm{dd}}^{\mathrm{a}}} E_{\mathrm{s}}^{\mathrm{o}} \cos\theta_{s} \tag{2}$$

$$E_{\mathrm{tot}} = E_{\mathrm{sun}} + E_{\mathrm{sky}} \tag{3}$$

$$E_{\mathrm{upw}} = \overline{r_{\mathrm{sd}}^{*}} E_{\mathrm{sun}} + \overline{r_{\mathrm{dd}}^{*}} E_{\mathrm{sky}} \tag{4}$$

$$r_{\mathrm{o}} = \frac{r_{\mathrm{so}}^{*} E_{\mathrm{sun}} + r_{\mathrm{do}}^{*} E_{\mathrm{sky}}}{E_{\mathrm{tot}}} \tag{5}$$

$$\pi L_{\mathrm{o}}^{\mathrm{TOA}} = \rho_{\mathrm{so}}^{\mathrm{a}} E_{\mathrm{s}}^{\mathrm{o}} \cos\theta_{\mathrm{s}} + \tau_{\mathrm{do}}^{\mathrm{a}} E_{\mathrm{upw}} + \tau_{\mathrm{oo}}^{\mathrm{a}} r_{\mathrm{o}} E_{\mathrm{tot}} \tag{6}$$

In above equations, $E_{\mathrm{s}}^{\mathrm{o}}$ is the extraterrestrial solar irradiance on a horizontal plane for the given solar zenith angle, and the six effective atmospheric parameters are described by:

$\tau_{\mathrm{ss}}^{\mathrm{a}}$	direct atmospheric transmittance for solar radiation
$\tau_{\mathrm{sd}}^{\mathrm{a}}$	diffuse atmospheric transmittance for solar radiation
$\rho_{\mathrm{dd}}^{\mathrm{a}}$	spherical albedo of the atmosphere
$\rho_{\mathrm{so}}^{\mathrm{a}}$	atmospheric bi-directional reflectance, or path reflectance
$\tau_{\mathrm{do}}^{\mathrm{a}}$	diffuse atmospheric transmittance in direction of viewing
$\tau_{\mathrm{oo}}^{\mathrm{a}}$	direct atmospheric transmittance in direction of viewing

The above quantities can be determined by an "interrogation" technique from successive MODTRAN4 (Berk et al., 2000) runs

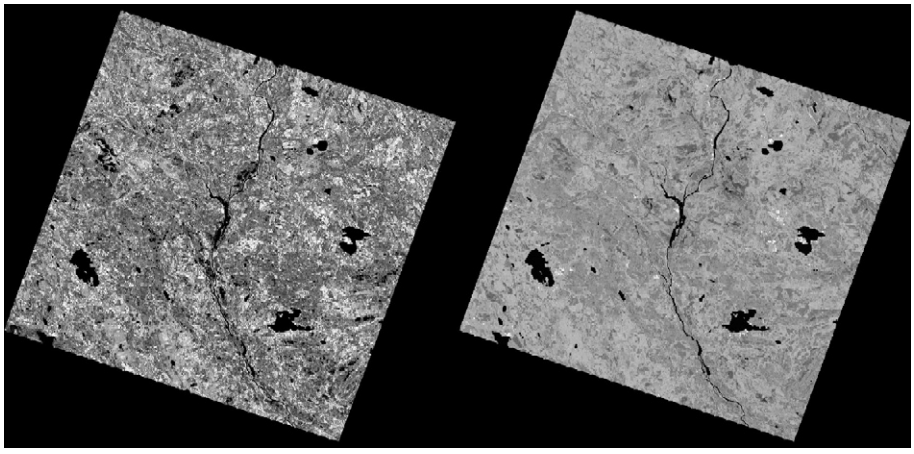

Fig. 9. Images of fAPAR (scaled between 0.5 and 1.0, left) and surface albedo (scaled between 0 and 0.275, right) for the Sodankylä site in Finland, based on coupled radiative transfer modeling of SLC and MODTRAN4. The images have been generated from simulations of the SPECTRA mission, and measure approx. 50×50 km^2 at 50 m spatial resolution.

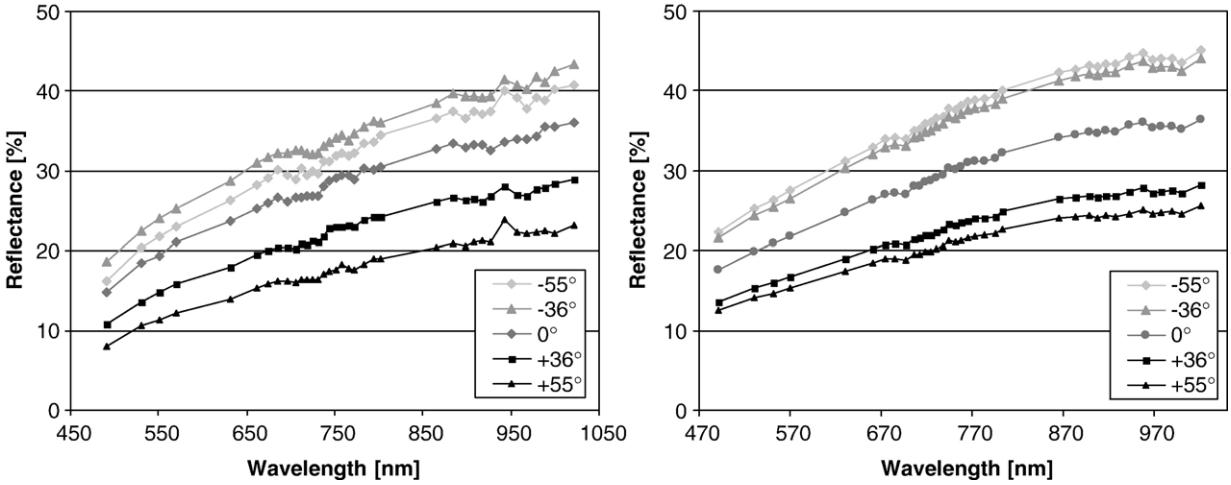

Fig. 10. Measured reflectance spectra for bare soil obtained by CHRIS for 5 observation angles (left) compared to SLC simulation results. Date 3 Aug. 2003, solar zenith: 32°, relative azimuth: 146.3° (forward looking), 33.7° (backward looking).

for three values of the surface albedo, as described in Verhoef and Bach (2003). The remaining quantities occurring in Eqs. (1)–(6) and not already defined earlier are:

E_{sun} solar irradiance at ground level
E_{sky} sky irradiance at ground level
E_{tot} total irradiance at ground level
E_{upw} diffuse upwelling irradiance from the ground, including surroundings
$\overline{r^*_{\mathrm{sd}}}$ spatially filtered hemispherical surface reflectance for solar incident flux
$\overline{r^*_{\mathrm{dd}}}$ spatially filtered bi-hemispherical surface reflectance
r_{o} directional reflectance factor (DRF) measured at ground level
$L_{\mathrm{o}}^{\mathrm{TOA}}$ top-of-atmosphere (TOA) radiance in the direction of viewing

Coupling of a surface reflectance model like SLC with an atmospheric model is essential to obtain simulations of surface directional reflectance and TOA radiance under realistic circumstances. An example of TOC (top-of-canopy) and TOA radiance spectra for a high spectral resolution of 1 nm and computed by the combination of the models 4SAIL and MODTRAN4 is shown in Fig. 7. This example is for a dense homogeneous canopy with an LAI of 4, spherical LIDF, bare soil surroundings, nadir viewing, a solar zenith angle of 30° and 23 km visibility. It illustrates the large impact of atmospheric scattering on radiances in the shortwave visible part of the spectrum and of water vapor absorption in the region between 800 and 1000 nm.

2.5. Calculation of fAPAR and albedo

Albedo and fAPAR (fraction absorbed photosynthetically active radiation) are important quantities for energy balance studies and input for crop growth models and estimation of evapotranspiration. As these quantities depend on the spectral distribution of the incident fluxes as well as on the reflective properties of the object, coupling hyperspectral surface reflectance models to atmospheric models is very useful since it enables accurate integrations over the associate spectral ranges. Apart from algorithms based on spectral indices like the NDVI, there are also more advanced methods to estimate fAPAR (Knyazikhin et al., 1998) and since model inversion techniques allow estimation of all basic canopy variables, forward modeling at hyperspectral resolution can next be applied to estimate fAPAR as follows.

By means of the canopy layer absorptances calculated as output of 4SAIL2, the absorbed radiation flux density (A) at a certain wavelength can be expressed by

$$A = \alpha^*_{\mathrm{s}} E_{\mathrm{sun}} + \alpha^*_{\mathrm{d}} E_{\mathrm{sky}}.$$

The fraction APAR is now found by integrating this expression over the PAR wavelength region (400–700 nm)

Table 5
Optical leaf and soil parameters used in SLC for the CHRIS simulations (NA stands for not applicable

Landuse	Maize	Deciduous forest
N green leaves	1.48	2
C_{ab} green leaves	58	60
C_{w} green leaves	0.02	0.009
C_{dm} green leaves	0.005	0.005
C_{s} green leaves	0	0.2
N brown leaves	2	NA
C_{ab} brown leaves	0	NA
C_{w} brown leaves	0	NA
C_{dm} brown leaves	0.01	NA
C_{s} brown leaves	0.7	NA
LIDF a	Varies with phenology	−0.20
LIDF b	Varies with phenology	−0.30
D	0.8	NA
Hot-spot size $s_{\mathscr{l}}$	varies with LAI	0.05
Tree shape ξ	NA	0.5
Soil Hapke b	0.84	NA
Soil Hapke c	0.68	NA
Soil Hapke B_0	0.30	NA
Soil Hapke h	0.23	NA

For forest *e.g.* this is the case, since no brown leaves are assumed in these simulations.
For maize $s_{\mathscr{l}}$ varies with LAI).

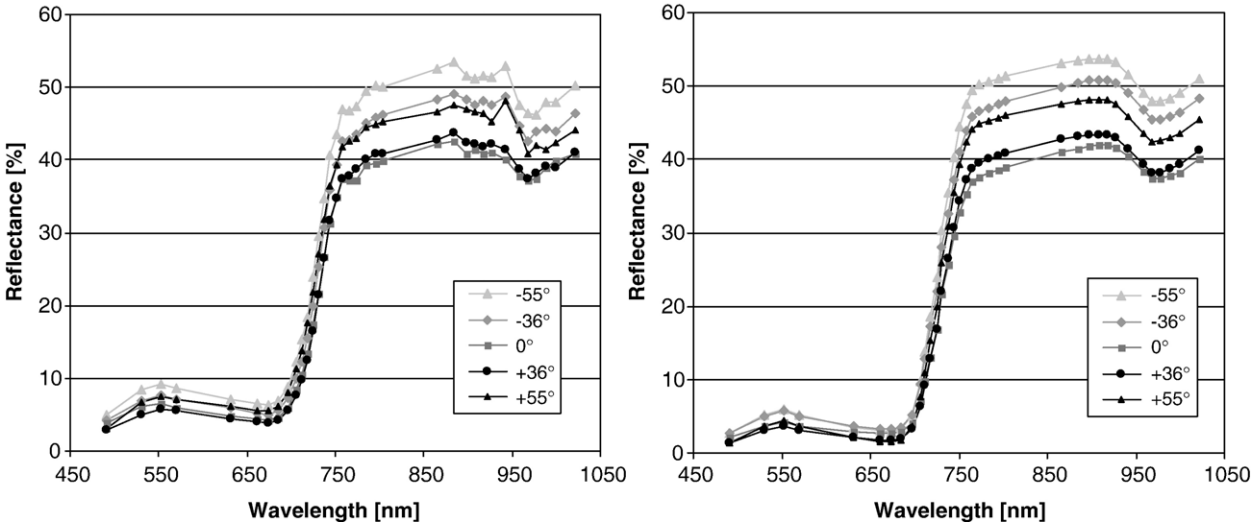

Fig. 11. Measured (left) and simulated (right) reflectance spectra for maize obtained by CHRIS for 5 observation angles. Date 3 Aug. 2003, solar zenith: 32°, relative azimuth: 146.3° (forward looking), 33.7° (backward looking).

and dividing by the total incident flux over the same wavelength range. This gives

$$f_{\mathrm{APAR}} = \frac{\sum_{400}^{700} A}{\sum_{400}^{700} E_{\mathrm{tot}}} = \frac{\sum_{400}^{700} (\alpha_{\mathrm{s}}^{*} E_{\mathrm{sun}} + \alpha_{\mathrm{d}}^{*} E_{\mathrm{sky}})}{\sum_{400}^{700} E_{\mathrm{tot}}} \tag{7}$$

In most cases a spectral sampling interval of 10 nm will be sufficiently accurate for most applications.

The surface albedo is the spectrally integrated hemispherically reflected flux divided by the spectrally integrated total incident flux. The hemispherically reflected flux at the top of the canopy is given by

$$E_{\mathrm{hem}} = r_{\mathrm{sd}}^{*} E_{\mathrm{sun}} + r_{\mathrm{dd}}^{*} E_{\mathrm{sky}}$$

so that the surface albedo (alb) is given by

$$\mathrm{alb} = \frac{\sum_{400}^{2400} E_{\mathrm{hem}}}{\sum_{400}^{2400} E_{\mathrm{tot}}} = \frac{\sum_{400}^{2400} (r_{\mathrm{sd}}^{*} E_{\mathrm{sun}} + r_{\mathrm{dd}}^{*} E_{\mathrm{sky}})}{\sum_{400}^{2400} E_{\mathrm{tot}}}. \tag{8}$$

Here the integration interval over the solar spectrum was limited to the range between 400 and 2400 nm, as this

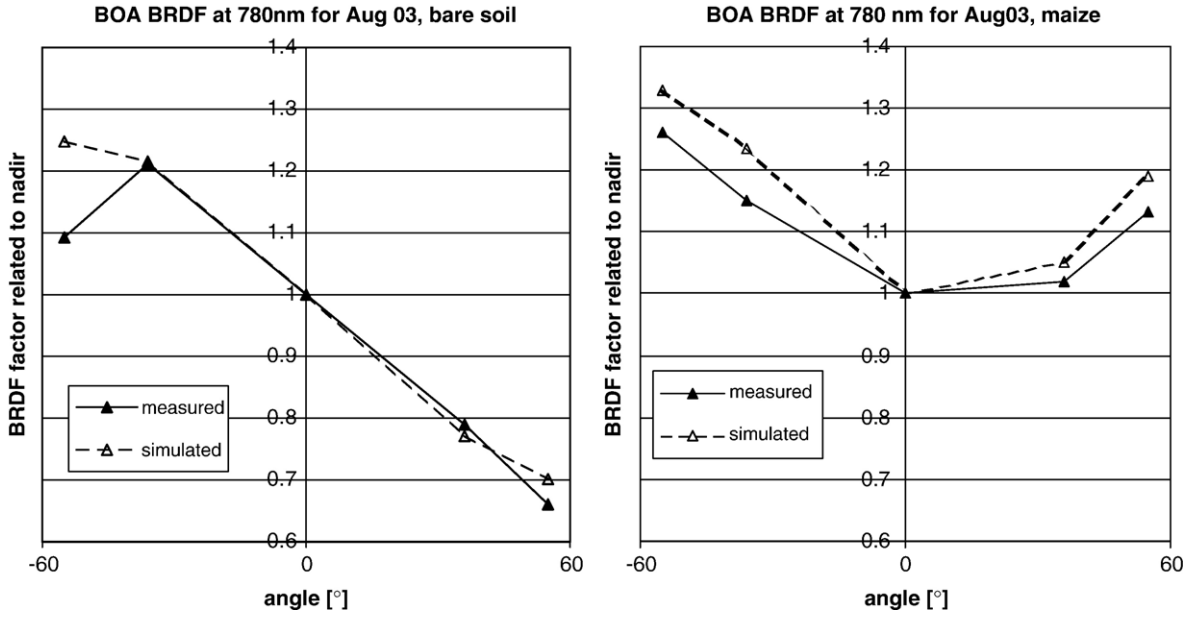

Fig. 12. Relative change of the reflectance at 780 nm with observation angle (Bottom of Atmosphere BRDF), measured with CHRIS and simulated with SLC for bare soil (left) and maize (right) on 3 Aug 2003.

represents the major part of the solar reflection regime. Also in this case a spectral sampling interval of 10 nm will be more than adequate to obtain an accurate estimate. In this respect it should be noted that optical sensors with incomplete spectral coverage and lower spectral resolution might be used to retrieve the most relevant object parameters by model inversion techniques, after which one can apply the models in forward direction over the complete solar spectrum and at hyperspectral resolution in order to obtain accurate estimates of fAPAR and surface albedo.

3. Examples

3.1. Three hot spots

BRDF profiles in the principal plane generated with the integrated model SLC should at least show two hot spot effects: the first is the one included in the Hapke-type soil BRDF model, and the second the one related to the canopy foliage. The first is mostly so wide that it will hardly be recognized as a hot spot, the second is usually quite narrow. In thin canopies one would expect to see a mixture of both types of hot spot effect. However, due to crown clumping, the shadowing of crowns on the soil background could create a kind of hot spot as well, perhaps of medium width, since crowns have quite large shadows. In order to demonstrate these BRDF effects in the principal plane, a simulation has been performed with SLC for a constant crown LAI of 4, a spherical LIDF and a varying crown cover from 0% to 100%, in steps of 25%. The results are plotted in Fig. 8 for a wavelength in the visible red at 670 nm. A logarithmic reflectance scale was chosen in order to emphasize relative differences. From the results it appears that at zero cover we see the soil BRDF with a very wide and faint hot spot. Next, increasing cover produces decreasing reflectances, first especially at large viewing zenith angles, later also at smaller angles. For intermediate crown cover (50%) this gives a moderately sharp hot spot effect related to crown shadowing, with a sharp peak superimposed on it due to the foliage. At complete crown cover only the very sharp hot spot peak related to the foliage remains. These simulation results indicate that BRDF profiles in the principal plane contain information on canopy structure on various scales. In this particular model abstraction, only two scales are involved, foliage and crowns, but in reality there may be more (needles, shoots, branches, crowns), thus creating a mixture of hot spots of increasing width.

3.2. Images of fAPAR and surface albedo

In an ESA study aimed at validating the former candidate hyperspectral multidirectional Earth Explorer mission SPECTRA, a numerical experiment was carried out to create artificial imagery for the Sodankylä boreal forest site in Finland. For this, a Landsat TM image was taken as input for a simple look-up table driven model inversion, and next the resulting biophysical maps were used as input for SLC in forward direction to produce artificial SPECTRA data (201 spectral bands in 7 directions). As a by-product, the SLC model was also used to compute accurate (in a numerical sense) images of fAPAR and surface albedo by employing the methods of Section 2.5. These data can further be employed to validate retrieval algorithms for these products. The results for fAPAR and surface albedo are presented in Fig. 9. The black parts are lakes, having no fAPAR and a very low albedo. The left image also shows some very dark patches of bare soil which have no fAPAR either, but they do have an albedo comparable to that of vegetation, as shown on the right image. In general the correlation between both products is low, indicating that they contain complementary information, although in this region albedo variations are rather modest anyway. The valid image area contains 1000×1000 scene pixels, and in order to generate the corresponding hyperspectral multi-angular SPECTRA data (201 spectral bands under 7 directions) 1407 million calls to the SLC model have been executed. Yet this task was accomplished in less than 6 h, thanks to the speed optimizations in SLC, taking advantage of the efficient handling of hyperspectral model calculations. This demonstrates that SLC can be applied in image processing environments and that its high speed allows its application in large scale model inversion exercises.

4. Validation

A validation of the SLC model was performed through comparison of simulation results with hyperspectral multidirectional measurements acquired by the CHRIS (Compact High Resolution Imaging Spectrometer) sensor. CHRIS is the first multi-angular, high spatial resolution imaging spectrometer in space, carried on board a platform called PROBA (Barnsley et al., 2004).

4.1. CHRIS hyperspectral data of the Upper Rhine Valley

4.1.1. The CHRIS-sensor

A specific feature of CHRIS is that it allows the acquisition of images at five observation angles (±55°, ±36° and near-nadir viewing) with high spatial resolution during one data take. This is important for the observation of the bi-directional reflectance distribution function (BRDF) of different land surfaces. CHRIS measures the reflected radiances over the visible and near infrared spectral range (400 to 1050 nm) with up to 63 spectral bands with approximately 10 nm width. In the selected spectral-spatial mode, the spatial resolution of the CHRIS images is 18 m at nadir view. It deteriorates by approximately a factor of two at the ±55° observation angles. This is still high enough for the observation of homogeneous canopies, reducing the problem of mixed pixels.

4.1.2. Test-site and basic processing steps

The test-site for this study was located in the Upper Rhine Valley, West of the City of Freiburg at 7.68° East and 48.19° North along the German–French border. Its average height above sea level is 150 m. The Upper Rhine Valley is a region of intensive agricultural use. One of the most important crops in the area is maize. Other crops grown are wheat and barley, as

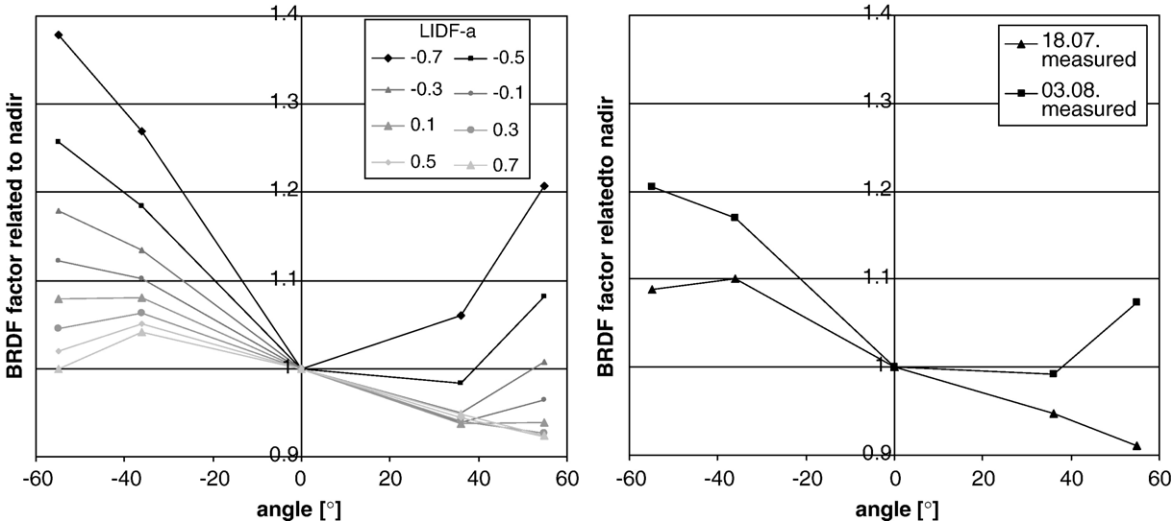

Fig. 13. Simulated BRDF factor at 780 nm related to nadir for a maize field with an LAI of 3.5 and its change with the canopy structure parameter LIDFa (left), compared with two BRDF signatures for maize measured by CHRIS on July 18 and August 3 (right).

well as special cultures, such as tobacco. Alluvial deciduous forests span along the riverside of the Rhine. Two cloud-free CHRIS acquisitions, from July and August 2003, could be used for the analyses.

Extensive processing of the raw CHRIS images was conducted. A statistical spatial destriping algorithm was applied in order to reduce the effects of detector non-uniformity. An atmospheric correction scheme called PULREF (Bach, 1995) using the radiative transfer model MODTRAN4 (Berk et al., 2000) was carried out to compensate for the scattering and absorption effects of the atmosphere and to obtain calibrated surface reflectances. The atmospheric correction included a correction of the adjacency effect. As a last step, the images were georectified using ground control points and standard image processing tools. The results of the correction are a set of co-registered and geo-referenced images containing the spectral and angular reflectance properties and their change with time.

4.2. Validation of SLC simulations using CHRIS measurements

BRDF functions of different land uses were analyzed visually and a comparison between measured reflectances of CHRIS data and simulated reflectances of the canopy reflectance model SLC has been performed. Since the soil determines the background reflectance of canopies and since the soil BRDF model was newly integrated in SLC, the validation starts with bare soil reflectances (Fig. 10). The SLC model parameters used to characterize the soil BRDF are listed in Table 5.

Qualitative interpretation of the bottom-of-atmosphere reflectances from all 5 observation angles of CHRIS showed that for bare soil, the nadir spectrum lies in the middle between the forward and backward (negative) looking angles (Fig. 10, left). The images at angles −55° and −36° are closer to the hot spot, and therefore brighter than the nadir spectrum. The angles

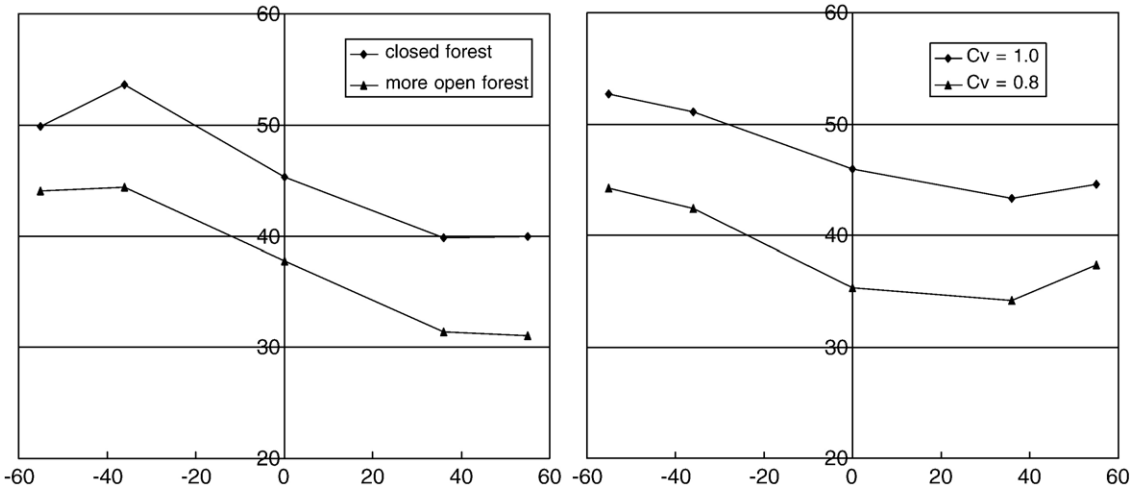

Fig. 14. Simulated BRDF at 780 nm for two types of forests with a LAI of 5; CHRIS measurements of Aug 3 (left) compared to SLC simulation results with varying C_v-values (right).

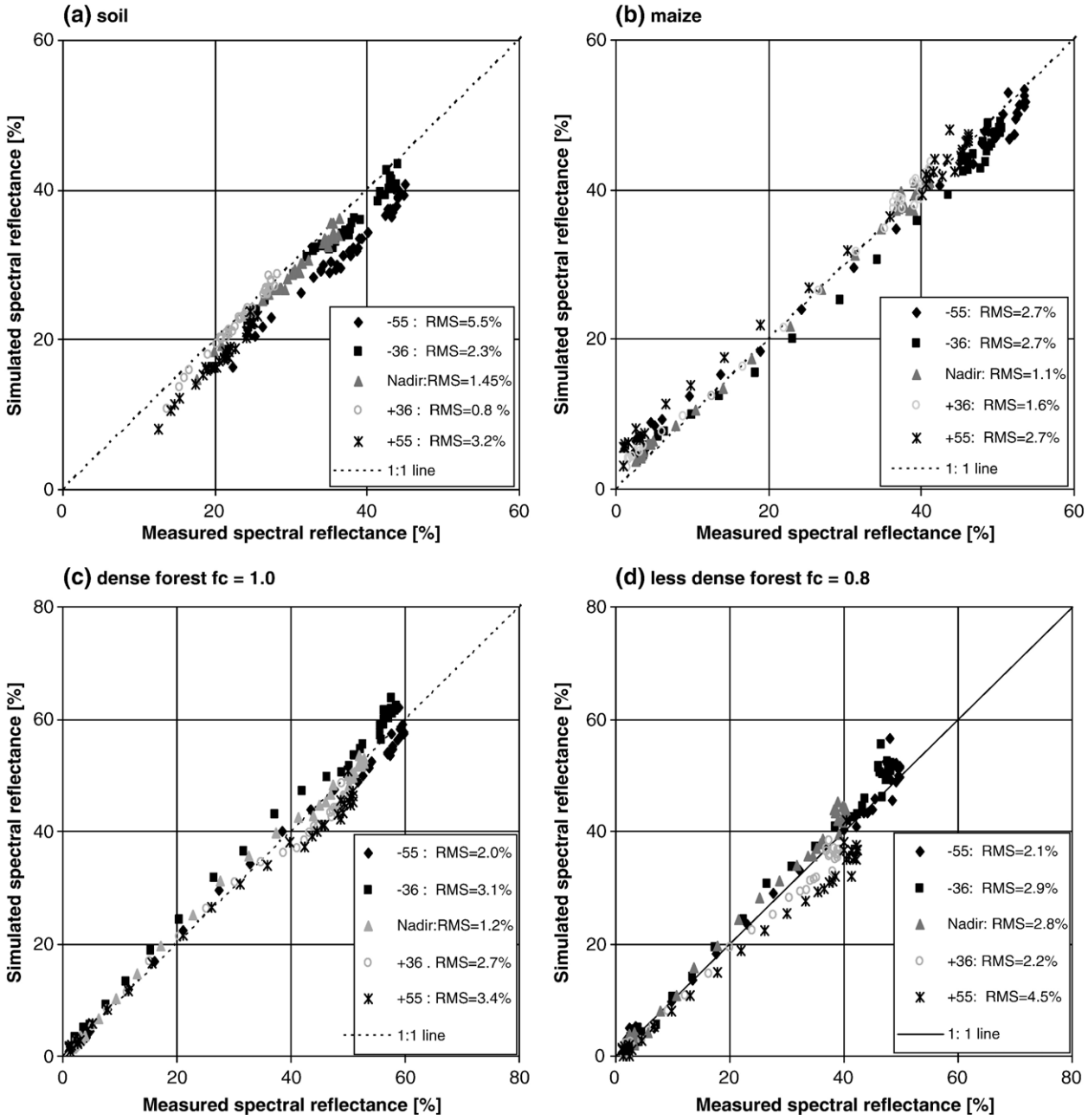

Fig. 15. Comparison of measured and simulated CHRIS observations and RMS difference for (a) soil, (b) maize, (c) dense forest and (d) less dense forest. Date 3 Aug. 2003, solar zenith: 32°, relative azimuth: 146.3° (forward looking), 33.7° (backward looking).

+55° and +36° are in directions more opposite to the sun and give darker images, since forward scattering is weaker than backscattering. Fig. 10 shows spectra for bare soil, measured and simulated, for August 3. The brightest measured spectrum is the −36° acquisition, closely followed by the −55° acquisition. For the simulated spectra, a volumetric soil moisture content of 5% was assumed, as there was no precipitation during the days before the acquisition and the summer of 2003 had been very dry. The agreement between the measured and simulated spectra is good for the nadir and the +36° spectra. The −55° spectrum is not represented quite as well. The measured −36° spectrum has higher reflectance values than the −55° spectrum, while the opposite is observable for the simulated spectrum (Fig. 10, right). In general, the soil BRDF model could fairly well represent the measurements of CHRIS.

A similar comparison between measured and simulated spectra was conducted for maize for the same acquisition date, August 3, and is illustrated in Fig. 11. For the simulation, canopy parameters were optimized from the nadir spectrum. This resulted in an LAI of 4.0, a chlorophyll content of 40 μg/cm^2, a fraction of brown leaves of 25% and a leaf water content of 0.02 g/cm^2. Compared to the nominal values of optical properties of maize (see Table 5), the chlorophyll content only had to be reduced slightly. Maize started to mature during August 2003, and as confirmed by field photos, it is plausible

that 25% of the maize leaves had turned brown already. There is a good agreement between CHRIS measurements and SLC simulations, though the simulated values seem to be too low in the visible spectral range (450–680 nm). This might be due to the blossoming of maize, an effect which cannot be accommodated easily in the SLC model.

Fig. 12 shows the same reflectances, retrieved from the August 3 CHRIS acquisitions, but this time at a fixed wavelength (780 nm) and with varying observation angle. The reflectance values are normalized to the nadir observations in order to emphasize BRDF effects. Also for the angular features, the SLC model agrees well with the measurements. For bare soil (Fig. 12, left) the most notable difference is again the decrease in reflectance for −55° in the measured values. For maize (Fig. 12, right) the shape of both BRDF functions (measured and simulated) is very similar, with a slight overestimation of the BRDF especially in the backward direction. The whole shape of the BRDF function for maize differs clearly from the bare soil function.

The canopy structure has a strong influence on the BRDF. This can be seen in Fig. 13 (left) for the SLC simulations results. In this sensitivity analysis, the BRDF function for various average leaf angles is represented in the parameter LIDFa of SLC. The BRDF function changes from roughly a bowl shape in the case of very vertical leaves (small LIDFa values) to a more or less linear shape with a maximum in the hot spot direction in the case of almost horizontal leaves (large LIDFa values). The measured BRDF function from CHRIS (Fig. 13, right) fits in with this very well.

The shape of the directional signature for the maize field on July 18 can be interpreted in such a way that this field is simulated best with an LIDFa parameter of approx. −0.1. For August 3 the LIDFa value changed to −0.5. This means that the average leaf angle increased from 49° to 63° during these two weeks, which is in line with the observed phenological development. This example also illustrates that it should be possible to retrieve indicators of canopy structure when inverting multi-angular observations.

Another extension of the presented SLC model is the consideration of the crown clumping for forests. How well can the integration of the C_v parameter represent the spectral and angular reflectance of forests with variable density? In order to study this, two forest sites were selected in the CHRIS image: one with a very dense deciduous forest and another with some gaps in the crowns that allow observation of the understorey at nadir view. The pixels in the CHRIS image were selected while avoiding mixed pixels. Mixed pixel effects are more likely for oblique views and forests consisting of high trees. A pixel was classified as homogeneous when the single pixel spectra were almost identical to the spectra after averaging the neighboring pixels (3×3 box).

The CHRIS measurements were again compared to SLC simulations. Since the investigated forests are very old and well developed, a crown LAI of 5 was assumed. Estimates from high resolution optical data resulted into complete crown coverage for the dense forest and a crown cover of approx. 80% in the less dense deciduous forest. Thus a C_v value of 0.8 could be assumed here. The understorey of this alluvial forest is wetland. Therefore a very dark background spectrum was assumed in the SLC simulations. Fig. 14 compares the measured and simulated BRDF of the reflectances at 780 nm. The reduction of the reflectance with reduced crown coverage is well captured by the model. The shape of the BRDF is sufficiently well represented.

As a summary of model performance for the CHRIS examples explained above, Fig. 15 shows the results plotted in the simulated-reflectance versus predicted-reflectance plane. Bare soil, maize and the two forest test-sites were plotted separately. The Root Mean Square (RMS) error quantifies the average deviation from the 1:1 line. This illustration is to give deviations between modeled and measured spectra as a function of the viewing direction. Therefore the different viewing directions are plotted with different symbols and the RMS is calculated for each view direction separately. For soil the backward 55° observation deviates most strongly from the 1:1 line with a general underestimation of the soil reflectance in the simulations. A similar behavior can be observed for the forward 55° observation of less dense forest, but for the other cases the scatter in the plots is fairly independent of the viewing angle. In general, the performance for the larger angles (±55°) is weaker than the performance for the ±36° angles, with RMS errors slightly increasing with observation angles. On average the RMS amounts to 1.6% for nadir viewing, 2.3% for ±36° and 3.3% for oblique observations with ±55°.

5. Discussion and conclusions

In the previous sections we have presented the integrated SLC model and demonstrated the power, versatility and relative simplicity of four-stream radiative transfer theory to construct comprehensive models of remote sensing observations of soil-vegetation objects from space. This enables investigating the relations between the biophysical properties of soils, leaves, vegetation canopy and the atmosphere on one hand, and remotely sensed TOA radiance spectra on the other, thus enhancing the insight in remote sensing applications and creating possibilities for improving methods of retrieval of quantitative information from earth observation data. The integrated model SLC is an example of a coupled soil–leaf-canopy radiative transfer model which is meant to be suitable for a broad variety of soil-vegetation objects, including forests. Unlike predecessors like PROSAIL, which is a combination of PROSPECT with SAILH (Bacour et al., 2002) resting on a Lambertian soil background, the SLC model incorporates a soil BRDF model, a modified version of the Hapke model. In addition, this soil model is able to capture the spectral effects of soil moisture variations all over the solar reflective spectral domain. Knowledge about the reflectance of the soil background or the understorey in a forest is very important for the accurate retrieval of vegetation properties from spectro-directional earth observation data by model inversion, since the uncertainty about the background has to be translated into a correspondingly larger variation in canopy properties. This is because more combinations of soil and canopy properties will be able to explain the observations if background uncertainty is large.

The canopy part of the model is 4SAIL2, a two-layer version of SAIL, which takes eight structural canopy parameters as input. This may seem a large number, but some of these parameters have only a minor impact on the observations, like for instance the layer dissociation factor. However, for all parameters there are conditions thinkable under which they will have a strong influence on observations. For instance, under large viewing angles, and at wavelengths where spectral differences between green and brown leaves are large, the layer dissociation factor may have a large impact. The tree shape factor is another parameter with mostly a small impact on modeled observations, but under special conditions (*e.g.* for an open forest observed close to the hot spot) this might be different. The 4SAIL2 model is numerically robust and also functions under conservative scattering conditions. Vertical heterogeneities in the form of leaf color gradients, as well as horizontal heterogeneities related to crown clumping, are accommodated in order to obtain realistic simulation results with a minimum number of parameters. Speed optimizations and the implementation as a Windows DLL guarantee a high throughput and a good potential for retrieval of quantitative information from earth observation data by model inversion techniques under operational conditions.

Coupling of the SLC model with the atmosphere is facilitated by the four-stream adding algorithm, which not only allows to compute top-of-atmosphere radiances, but also solar and sky irradiance spectra on ground level, thus enabling the accurate computation of fAPAR and surface albedo. An interactive demo application has been built in the Visual Basic 5 language which is suitable for educational purposes and for the manual fitting of model-calculated spectra to observations.

In the validation section the SLC model was fitted to CHRIS-PROBA data of the Upper Rhine Valley in Germany to demonstrate that observed spectral-directional data from bare soil, maize and forest could be reproduced by the model fairly well, in spite of the limited availability of ground data. The deviation of the model was in a first approximation assessed using the RMS error between measured and simulated reflectances, which resulted in good correspondence with RMS values slightly increasing with larger observation angles. A formal model inversion and accuracy assessment was not attempted yet, since ground truth data were unfortunately mostly lacking for the used CHRIS data set. These tests are presently undertaken with CHRIS observations of the years 2005 and 2006 acquired over a precision farming test-site in the eastern part of Germany (Begiebing et al., 2006). We showed that for maize the LIDF parameters *a* and *b* have a significant impact on directional signatures of the reflectance, and that it was even possible to "measure" a temporal change of the LIDF (leaf slope) in a couple of weeks between two satellite image acquisitions.

Acknowledgements

The SLC model was developed in the frame of two ESA studies related to the Earth Explorer Mission SPECTRA, under ESTEC contracts 17169 and 17179, with additional support from NLR's own research programme. The SLC validation activities were additionally supported within the BMBF project preagro (FK 0330679). The provision of CHRIS data by ESA and SIRA is acknowledged. Many thanks to Silke Begiebing for the CHRIS data processing. Three anonymous reviewers provided numerous suggestions for improvement of the final manuscript.

Appendix A. Four-stream adding equations for a canopy layer resting on a non-Lambertian soil background

Starting with the four basic soil reflectance factors r_{so}, r_{do}, r_{sd} and r_{dd} computed by the soil BRDF model, the eleven optical quantities of the canopy layer listed in Table 2 are used to calculate the four resulting top-of-canopy reflectance factors as follows:

$$r^*_{so} = \rho_{so} + \tau_{ssoo} r_{so} + \frac{(\tau_{ss} r_{sd} + \tau_{sd} r_{dd})\tau_{do} + (\tau_{sd} + \tau_{ss} r_{sd} \rho^b_{dd}) r_{do} \tau_{oo}}{1 - r_{dd} \rho^b_{dd}} \quad (A.1)$$

$$r^*_{do} = \rho_{do} + \frac{\tau_{dd}(r_{dd}\tau_{do} + r_{do}\tau_{oo})}{1 - r_{dd}\rho^b_{dd}} \quad (A.2)$$

$$r^*_{sd} = \rho_{sd} + \frac{(\tau_{ss} r_{sd} + \tau_{sd} r_{dd})\tau_{dd}}{1 - r_{dd}\rho^b_{dd}} \quad (A.3)$$

$$r^*_{dd} = \rho^t_{dd} + \frac{\tau_{dd} r_{dd} \tau_{dd}}{1 - r_{dd}\rho^b_{dd}} \quad (A.4)$$

Based on the absorptances of the isolated canopy layer for solar and hemispherical diffuse incident flux, α_s and α_d (which are computed within 4SAIL2), these are modified to include the soil background reflectance as follows:

$$\alpha^*_s = \alpha_s + \frac{\tau_{ss} r_{sd} + \tau_{sd} r_{dd}}{1 - r_{dd}\rho^b_{dd}} \alpha_d \quad (A.5)$$

$$\alpha^*_d = \alpha_d + \frac{\tau_{dd} r_{dd}}{1 - r_{dd}\rho^b_{dd}} \alpha_d \quad (A.6)$$

where $\alpha_s = 1 - \rho_{sd} - \tau_{sd} - \tau_{ss}$ and $\alpha_d = 1 - \rho_{dd} - \tau_{dd}$ are the absorptances of the isolated canopy layer for solar and diffuse incident flux, respectively.

References

Allen, W. A., Gayle, T. V., & Richardson, A. J. (1970). Plant canopy irradiance specified by the Duntley equations. *Journal of the Optical Society of America*, *60*(3), 372–376.

Asrar, G., Myneni, R. B., & Choudhury, B. J. (1992). Spatial heterogeneity in vegetation canopies and remote sensing of absorbed photosynthetically active radiation: A model study. *Remote Sensing of Environment*, *41*, 85–103.

Atzberger, C. (2000, June 14–16). Development of an invertible forest reflectance model: The INFOR Model. In Buchroithner (Ed.), *A decade of trans-European remote sensing cooperation. Proc. 20th EARSeL Symposium, Dresden, Germany* (pp.39–44).

Bach, H. (1995). Die Bestimmung hydrologischer und landwirtschaftlicher Oberflächenparameter aus hyperspektralen Fernerkundungsdaten (The

determination of hydrological and agricultural land surface parameters from hyperspectral remote sensing data.), PhD Thesis, Münchener Geographische Abhandlungen 21, 175 p.

Bach, H., & Mauser, W. (1994). Modelling and model verification of the spectral reflectance of soils under varying moisture conditions. *Proc. IGARSS' 94 Symposium, Pasadena*, *Vol. 4*(pp.2354-2356).

Bacour, C., Jacquemoud, S., Tourbier, Y., Dechambre, M., & Frangi, J. P. (2002). Design and analysis of numerical experiments to compare four canopy reflectance models. *Remote Sensing of Environment*, *79*, 72−83.

Barnsley, M. J., Settle, J. J., Cutter, M., Lobb, D., & Teston, F. (2004). The PROBA/CHRIS mission: A low-cost smallsat for hyperspectral multiangle observations of the earth surface and atmosphere. *IEEE Transactions on Geoscience and Remote Sensing*, *42*(7), 1512−1520.

Begiebing, S., Bach, H., Wehrhan, M., & Mauser, W. (2006). Derivation of canopy parameters of wheat using hyperspectral, directional remote sensing data and the canopy reflectance model SLC. *Agricultural engineering for a better world – World Congress – incl. CD-ROM* Bonn: VDI-Tagungsband ISBN:3-18-091958-2.

Berk, A., Anderson, G. P., Acharya, P. K., Chetwynd, J. H., Bernstein, L. S., Shettle, E. P., et al. (2000). *MODTRAN4 USERS MANUAL, Air Force Research Laboratory, Space Vehicles Directorate, Air Force Materiel Command, Hanscom AFB, MA 01731-3010, USA.* 97 pp.

Bréon, F. -M., Maignan, F., Leroy, M., & Grant, I. (2002). Analysis of hot spot directional signatures measured from space. *Journal of Geophysical Research*, *107*, D16. doi:10.1029/2001JD001094

Chelle, M. (1997). Développement d'un modèle de radiosité mixte pour simuler la distribution du rayonnement dans les couverts végétaux. PhD thesis, Université de Rennes, 161 pp.

Combal, B., Baret, F., Weiss, M., Trubuil, A., Mace, D., Pragnère, A., et al. (2002). Retrieval of canopy biophysical variables from bidirectional reflectance: Using prior information to solve the ill-posed inverse problem. *Remote Sensing of Environment*, *84*(1), 1−15.

Dawson, T. P., Curran, P. J., & Plummer, S. E. (1998). LIBERTY-modelling the effects of leaf biochemistry on reflectance spectra. *Remote Sensing of Environment*, *65*, 50−60.

De Ruiter, J. F., Peters, S. W. M., Van de Griend, A. A., & Rosema, A. (1997). Monitoring boreal forest with Landsat TM: A validation of the Forest Light Interaction Model. *Techn. Rep.Fac. Earth Sciences*, *Vol. 1*. Amsterdam, The Netherlands: Vrije Universiteit, 29 pp.

Gastellu-Etchegory, J. P., Demarez, V., Pinel, V., & Zagolski, F. (1996). Modeling radiative transfer in heterogeneous 3-D vegetation canopies. *Remote Sensing of Environment*, *58*, 131−156.

Gemmell, F., & Varjo, J. (1999). Utility of reflectance model inversion versus two spectral indices for estimating biophysical characteristics in a boreal forest test site. *Remote Sensing of Environment*, *68*, 95−111.

Gerstl, S. A. W., & Borel, C. C. (1992). Principles of the radiosity method versus radiative transfer for canopy reflectance modeling. *IEEE Transactions on Geoscience and Remote Sensing*, *30*(2), 271−275.

Gobron, N., Pinty, B., Verstraete, M. M., & Govaerts, Y. (1997). A semi-discrete model for the scattering of light by vegetation. *Journal of Geophysical Research*, *102*, 9431−9446.

Goel, N. S. (1988). Models of vegetation canopy reflectance and their use in estimation of biophysical parameters from reflectance data. *Remote Sensing Reviews*, *4*, 1−212.

Hapke, B. W. (1981). Bi-directional reflectance spectroscopy 1. Theory. *Journal of Geophysical Research*, *86*, 3039−3054.

Huemmrich, K. F. (2001). The GeoSail model: A simple addition to the SAIL model to describe discontinuous canopy reflectance. *Remote Sensing of Environment*, *75*(3), 423−431.

Jacquemoud, S., & Baret, F. (1990). PROSPECT: A model of leaf optical properties spectra. *Remote Sensing of Environment*, *34*, 75−91.

Jasinski, M. F. (1996). Estimation of subpixel vegetation density of natural regions using satellite imagery. *IEEE Transactions on Geoscience and Remote Sensing*, *34*(3), 804−813.

Knyazikhin, Y. V., Marshak, A. L., & Myneni, R. B. (1992). Interaction of photons in a canopy of finite-dimensional leaves. *Remote Sensing of Environment*, *39*, 61−74.

Knyazikhin, Y., Martonchik, J. V., Myneni, R. B., Diner, D. J., & Running, S. W. (1998). Synergistic algorithm for estimating vegetation canopy leaf area index and fraction of absorbed photosynthetically active radiation from MODIS and MISR data. *Journal of Geophysical Research*, *103*, 32257−32274.

Kuusk, A. (1985). The hot spot effect of a uniform vegetative cover. *Soviet Journal of Remote Sensing*, *3*, 645−658.

Kuusk, A., & Nilson, T. (2000). A directional multispectral forest reflectance model. *Remote Sensing of Environment*, *72*, 244−252.

Le Maire, G., François, C., & Dufrêne, E. (2004). Towards universal broad leaf chlorophyll indices using PROSPECT simulated database and hyperspectral reflectance measurements. *Remote Sensing of Environment*, *89*, 1−28.

Li, X., Strahler, A. H., & Woodcock, C. E. (1995). A hybrid geometric optical radiative transfer approach for modeling albedo and directional reflectance of discontinuous canopies. *IEEE Transactions on Geoscience and Remote Sensing*, *33*, 466−480.

Nicodemus, F. E. (1970). Reflectance nomenclature and directional reflectance and emissivity. *Applied Optics*, *31*(36), 7669−7683.

Nilson, T., & Kuusk, A. (1989). A reflectance model for the homogeneous plant canopy and its inversion. *Remote Sensing of Environment*, *27*, 157−167.

North, P. R. J. (1996). Three-dimensional forest light interaction model using a Monte Carlo method. *IEEE Transactions on Geoscience and Remote Sensing*, *34*, 946−956.

Pinty, B., Verstraete, M. M., & Dickinson, R. E. (1989). A physical model for predicting bi-directional reflectances over bare soil. *Remote Sensing of Environment*, *27*, 273−288.

Pinty, B., Widlowski, J. -L., Taberner, M., Gobron, N., Verstraete, M. M., Disney, M., et al. (2004). Radiation Transfer Model Intercomparison (RAMI) exercise: Results from the second phase. *Journal of Geophysical Research*, *109*, D06210. doi:10.1029/2003JD004252

Rosema, A., Verhoef, W., Noorbergen, H., & Borgesius, J. J. (1992). A new forest light interaction model in support of forest monitoring. *Remote Sensing of Environment*, *42*, 23−41.

Schlerf, M., & Atzberger, C. (2006). Inversion of a forest reflectance model to estimate structural vegetation attributes using hyperspectral remote sensing data. *Remote Sensing of Environment*, *100*, 281−294.

Shultis, J. K., & Myneni, R. B. (1988). Radiative transfer in vegetation canopies with anisotropic scattering. *Journal of Quantitative Spectroscopy & Radiative Transfer*, *39*, 115−129.

Smolander, S., & Stenberg, P. (2003). A method to account for shoot scale clumping in coniferous canopy reflectance models. *Remote Sensing of Environment*, *88*, 363−373.

Suits, G. H. (1972). The calculation of the directional reflectance of a vegetative canopy. *Remote Sensing of Environment*, *2*, 117−125.

Thompson, R. L., & Goel, N. S. (1998). Two models for rapidly calculating bidirectional reflectance: Photon spread (ps) model and statistical photon spread (sps) model. *Remote Sensing Reviews*, *16*, 157−207.

Van de Hulst, H. C. (1980). *Multiple light scattering.* London: Academic.

Verhoef, W. (1984). Light scattering by leaf layers with application to canopy reflectance modeling: The SAIL model. *Remote Sensing of Environment*, *16*, 125−141.

Verhoef, W. (1985). Earth observation modeling based on layer scattering matrices. *Remote Sensing of Environment*, *17*, 165−178.

Verhoef, W. (1998). Theory of radiative transfer models applied in optical remote sensing of vegetation canopies, PhD Thesis, Wageningen Agricultural University, 310 pp.

Verhoef, W. (2002). Improved modeling of multiple scattering in leaf canopies: The model SAIL++. In J. A. Sobrino (Ed.), *Proc. 1st Int. Symp. on Recent Advances in Quantitative Remote Sensing* (pp. 11−20). Spain: Universitat de Valencia.

Verhoef, W., & Bach, H. (2003). Simulation of hyperspectral and directional radiance images using coupled biophysical and atmospheric radiative transfer models. *Remote Sensing of Environment*, *87*, 23−41.

Zarco-Tejada, P. J., Rueda, C. A., & Ustin, S. L. (2003). Water content estimation in vegetation with MODIS reflectance data and model inversion methods. *Remote Sensing of Environment*, *85*, 109−124.